JOURNAL OF CHEMICAL INFORMATION AND MODELING

Article

pubs.acs.org/jcim

Understanding the Inhibitory Effect of Highly Potent and Selective Archazolides Binding to the Vacuolar ATPase

Sandra Dreisigacker,[†,‡] Dorota Latek,[‡,§] Svenja Bockelmann,[∥] Markus Huss,[∥] Helmut Wieczorek,[∥] Slawomir Filipek,[⊥] Holger Gohlke,[#] Dirk Menche,[†,▽] and Teresa Carlomagno*[,‡]

[‡]Structural and Computational Biology Unit, EMBL, Mayerhofstrasse 1, D-69117 Heidelberg, Germany

[†]Institute of Organic Chemistry, Ruprecht-Karls University Heidelberg, Im Neuenheimer Feld 270, D-69120 Heidelberg, Germany

[∥]Department of Animal Physiology, Faculty of Biology and Chemistry, University of Osnabrück, Barbarastrasse 11, D-49069 Osnabrück, Germany

[⊥]Faculty of Chemistry, University of Warsaw, Pasteura 1, 02-093 Warsaw, Poland

[#]Heinrich-Heine-University Düsseldorf, Institute of Pharmaceutical and Medicinal Chemistry, Universitätsstrasse 1, D-40225 Düsseldorf, Germany

Supporting Information

ABSTRACT: Vacuolar ATPases are a potential therapeutic target because of their involvement in a variety of severe diseases such as osteoporosis or cancer. Archazolide A (**1**) and related analogs have been previously identified as selective inhibitors of V-ATPases with potency down to the subnanomolar range. Herein we report on the determination of the ligand binding mode by a combination of molecular docking, molecular dynamics simulations, and biochemical experiments, resulting in a sound model for the inhibitory mechanism of this class of putative anticancer agents. The binding site of archazolides was confirmed to be located in the equatorial region of the membrane-embedded V_O-rotor, as recently proposed on the basis of site-directed mutagenesis. Quantification of the bioactivity of a series of archazolide derivatives, together with the docking-derived binding mode of archazolides to the V-ATPase, revealed favorable ligand profiles, which can guide the development of a simplified archazolide analog with potential therapeutic relevance.

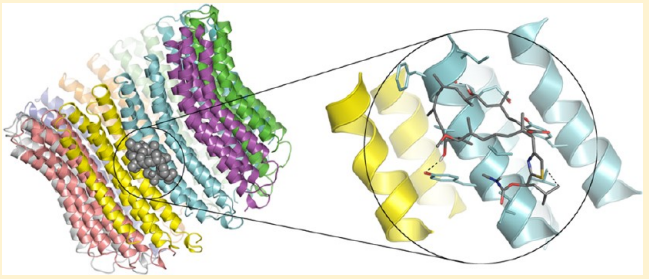

INTRODUCTION

The polyketide family of archazolides – isolated from myxobacteria *Archangium gephyra* and *cystobacter violaceus*[1−4] – are well-established natural products. In the past years, we reported on the structure elucidation and the first total synthesis of archazolide A (**1**) (Figure 1), and, more recently, on the syntheses of analogs and their bioactivity.[5−11] Archazolides are interesting molecules both from the structural point of view and in terms of their potential utility as pharmaceutical drugs. They display impressive biological properties, including potent cytotoxicity against several tumor cell lines in the subnanomolar range.[2−4,7] The cytotoxicity is attributed to the binding of archazolides to the vacuolar ATPase (V-ATPase), which leads to an inhibition of this vital enzyme. V-ATPases use the energy from ATP hydrolysis to translocate protons across membranes, thereby energizing secondary active transport processes or acidifying either the extracellular medium or the lumen of intracellular organelles.[12] Cleavage of ATP occurs at the cytosolic V_1-complex, while proton transport is mediated by the membrane-integral V_O-complex of the enzyme. The V_O-complex comprises a ring of c subunits. Each subunit contains a conserved glutamate residue that is essential for proton translocation.[13] V-ATPase mediated extracellular acidification contributes for example to bone resorption by osteoclasts or to metastasis of tumor cells. Accordingly, V-ATPases represent a potential target for the treatment of severe diseases such as osteoporosis or cancer.[14,15] The function of V-ATPase is effectively inhibited by archazolides, which bind selectively to the c subunits of the membrane-integral V_O-rotor.[7] In contrast, other ion translocating enzymes, e.g., F-type and P-type ATPases, are not affected by these inhibitors at concentrations up to 10 μM,[7] which makes archazolides highly interesting as prospective potent and selective therapeutic agents. Furthermore, archazolide F (**3**), with inhibitory profiles in the picomolar range, is the most active inhibitor of V-ATPase-controlled cell growth discovered so far (Figure 1) and also displays a 10-fold higher efficiency for human cell lines compared to its derivatives archazolide A (**1**) and B (**2**).[4]

The development of archazolides into new pharmaceuticals requires both easy accessibility of the substance and highly selective biological activity. Unfortunately, neither isolation nor total synthesis of archazolides accomplishes the amount of natural product that would be needed in a pharmaceutical

Received: May 23, 2012
Published: July 2, 2012

dx.doi.org/10.1021/ci300242d | J. Chem. Inf. Model. 2012, 52, 2265−2272

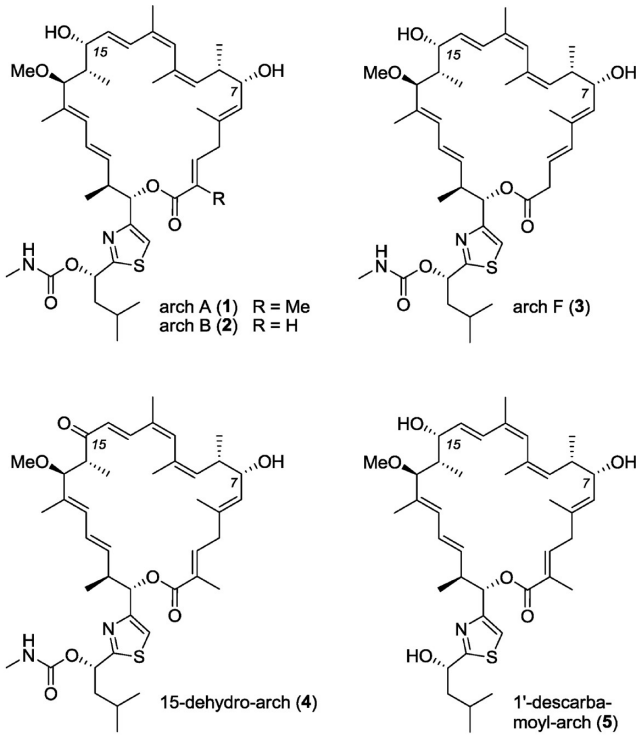

ligand	enzyme inhibition V_1/V_O holoenzyme IC_{50} [nmol/mg enzyme][a]	growth inhibition cell line L-929 IC_{50} [nM][c]
1	0.60[b]	0.81
2	0.60	1.10
3	0.70	0.10
4	13.0	>5000
5	5.00	14.0

Figure 1. Structures of natural archazolides A, B, F (**1**–**3**) and synthetic 15-dehydro-archazolide (**4**) and 1′-descarbamoyl-archazolide (**5**). Inhibition of the V_1/V_O holoenzyme activity and IC_{50} values on growth inhibition in mouse cell line L-929 are shown in the table.

context. This limitation calls for a simpler, easier-to-synthesize analog that retains all essential interactions of archazolides with the target protein. To this end, in this work we study the binding mode of archazolides to the V-ATPase with the goal of revealing the key structural features for the high activity of the natural product.

In previous work, we performed radioactive photoaffinity labeling of archazolide A (**1**) and proximate cross-linking studies with purified V-ATPase to identify the c-subunit of the rotor as target for archazolides.[11] Furthermore, we used ligand competition analyses and site-directed mutagenesis of the *S. cerevisiae* subunit c to characterize the binding site of archazolides in more detail.[11] We discovered that archazolide A (**1**) prevents the covalent binding of the inhibitor *N,N′*-dicyclohexylcarbodiimide (DCCD) to glutamate E137 within subunit c[11,16] and the binding of the plecomacrolide inhibitors at the interface between two adjacent c subunits.[7,17] Last but not least, we showed that in yeast the amino acid exchanges Y142N and L144I in subunit c lead to V-ATPases that bind ligand **1** 10-fold more efficiently than the wild-type protein.[11] These results indicated that the binding site of archazolides comprises, or is close to, amino acids E137, Y142, and L144 (amino acids positions according to yeast subunit c), located in the equatorial region of the rotor structure (Figure 2). However, the exact location and shape of the archazolide binding pocket remained unclear.

Here, we aim at describing the binding mode of archazolides to V-ATPase by a combination of biochemical experiments and docking calculations. First, we dock ligand **1** to a model of the V_O-ring formed by ten c subunits of *S. cerevisiae* to identify possible binding pockets and binding modes of archazolides to the rotor structure. Second, we select the pose that is best in agreement with the mutational analysis conducted in ref 11 and with the activity of archazolide analogs reported in refs 2–4. Third, we refine the selected binding pose in a membrane-like environment by molecular dynamics (MD) simulations in order to obtain a more realistic picture of the intermolecular interactions. Last, we verify the validity of our pose by measuring the bioactivity of archazolide derivatives with a yeast mutant V-ATPase, which confirmed the predictions made on the basis of the docked model. The binding pose of archazolides to the V-ATPase presented here reveals the features of the intermolecular interactions that are responsible for the high affinity of the ligand. These results are critical for further efforts of our and other laboratories aimed at designing a potent ligand based on the archazolide scaffold with an easily accessible synthetic route.

RESULTS AND DISCUSSION

The protein input structure for the docking calculations was prepared by homology modeling of the yeast c subunit using the crystallographic structure of the *E. hirae* rotor as template.[11] The two proteins display 35% (85%) sequence identity (similarity) in the equatorial region, which speaks for the validity of the homology model for docking studies (Figure S1). The amino acid sequence in the equatorial region is conserved also in other V-ATPase rotor subunits (Figure S2); in this work we choose to model the yeast c subunit to provide a direct comparison with the mutational analysis, which is performed on the yeast protein. To accelerate the docking calculations only three units of the decameric rotor were used (Figure S3). The whole rotor structure is stable during 10 ns of MD simulations conducted in an explicit membrane (Figure S4). To sample a larger conformational space of the binding pocket side chains, 22 protein structures were generated in a 1.1 ns MD run in aqueous solution (see Experimental Procedures for details). The (modest) variability of the side chains in the equatorial region of the rotor is shown in Figure S5. All 22 structures were used in ensemble docking calculations. The electrostatic potential of the archazolide binding site is shown in Figure S6.[18]

To minimize the uncertainties of the modeling results, we assumed that the bioactive conformation of the macrocycle of **1** is similar to that determined for free archazolide in solution by NMR (Figure S7).[6] This choice follows the rationale that the bioactive conformation of small molecules is usually highly populated in solution to minimize unfavorable energetic contributions upon binding.[19,20] In contrast, the carbamate side chain, the methoxy-, and the hydroxyl groups were left free to adapt to the protein binding region during docking (Figure S8). The initial structure of archazolide derivatives **1**–**4** were obtained by substitution of the corresponding functional groups in the solution structure of **1** followed by energy minimization.

dx.doi.org/10.1021/ci300242d | J. Chem. Inf. Model. 2012, 52, 2265–2272

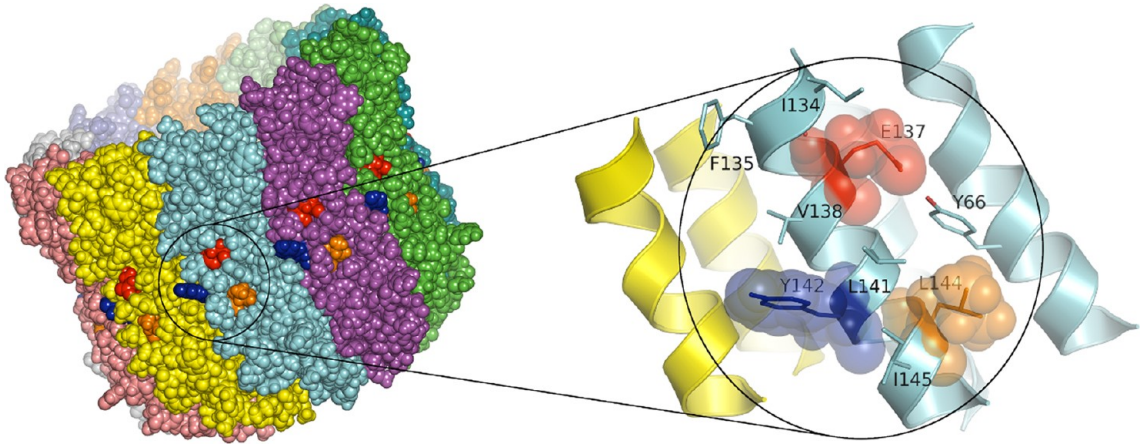

Figure 2. Left: Sphere representation of a decameric V_O-ring formed of *S. cerevisiae* c subunits. The c subunits, consisting of 4 transmembrane helices each, are shown in different colors. Residues involved in the binding of the V_O-ring to archazolides, identified in previous studies, are colored in red (E137), blue (Y142), and orange (L144), respectively. Right: Zoom of the protein region containing the critical residues, with E137, Y142, and L144 represented as spheres. Amino acids are labeled in one letter code.

This choice is justified by the high bioactivity of all derivatives (Figure 1), which would not be compatible with a major change of the interaction mode.

Next, we docked archazolide analogs **1**−**4** to the homology model of the yeast c-ring using the program Autodock3.0[21] together with Drugscore[22] as objective function (Figure S9 and S10). The resulting docking modes for each archazolide derivative to the 22 models of subunit c were clustered before analysis. Docking of archazolide A (**1**) to the homology model yielded five different binding poses **B1**−**B5** (Figure S11). **B2** represents the most populated cluster, followed by **B1** and **B5**. Both **B1** and **B5** display a twin pose, with the same binding mode for the macrocycle, but a different orientation of the side chain containing the thiazole ring; in the twin poses, the interaction partners of the methyl-carbamate and the *i*-butyl side chain are effectively switched. Of the five possible binding modes of **1** to the yeast c-ring, **B1**, **B3**, and **B4** can be safely excluded because in these poses the archazolide does not display any contacts to either Y142 or L144, which were identified to be part of the binding pocket by mutational analysis.[11] Therefore, in the following analysis, we consider **B2** and **B5** only (Figure 3).

Binding Pose B2. In **B2** the C17-OMe and the methyl groups at C2, C12, and C16 are in close proximity to I134, V138, Y142, L141, and L144, whereas the methyl groups at C5, C10, C22, and the hydroxyl group at C7 face the solvent and do not show any interactions with the protein surface. The hydroxyl group at C15 interacts with the polar side chains of E137 and Y66. In this position the ligand partially occupies the DCCD binding pocket, which would explain why archazolide binding prevents binding of DCCD (Figure S12A). The thiazole side chain penetrates a hydrophobic cleft formed by two adjacent subunits including residues T32, G61, I65, and L139. This tight interaction is likely responsible for the favorable binding energy of the complex. Notably, activity data for archazolides with a G61S mutant protein indicated no effect of this mutation on binding.[11] These data are thus contradictory to **B2**, from which a longer amino acid side chain at position 61 is predicted to partially obstruct the hydrophobic cavity and therefore impact ligand binding. Docking calculations performed with the G61S mutant protein supported this prediction, as the populations of the poses **B1**−**B3** drop considerably upon substitution of G61 with a serine (Figure S13). In addition, this pose does not easily recapitulate the poor bioactivity of archazolide C,[2] with a glucose moiety at the C7, as the hydroxyl group at this position is directed toward the solvent. All in all, this pose can explain only a limited set of bioactivity data for archazolide derivatives.

Binding Pose B5. In **B5** the methyl groups at C2, C5, C10, C12, and C16 are in close proximity to residues Y66, I134, F135, E137, V138, and L141, providing favorable hydrophobic interactions, whereas C22-Me is the only aliphatic group that is not directed toward the protein. The C1−C6 region of the ligand entertains hydrophobic interaction with Y66, well in agreement with the similar affinity of the Y66F mutant protein for archazolides as compared to the wild-type protein.[11] The C7-OH forms a hydrogen bond to the backbone of I134, again occupying the binding pocket of DCCD and thereby preventing its binding (Figure S12B). In addition, this binding pose is in good agreement with the low bioactivity of archazolide C,[2] as a glucose moiety at C7 would clash with the protein surface. The thiazole-bearing side chain contacts residues L141, L144, and I145, and, in contrast to pose **B2**, there is no interaction with G61. The C15-OH is close to residue Y142. If this residue is mutated to asparagine, the C15-OH could form a hydrogen bond with the carbonyl group, thus explaining the increased ligand activity with the Y142N mutant protein. In conclusion, this pose agrees well with all activity data of archazolides with both the wild type and the mutant proteins. Thus, we propose that binding mode **B5** (Figure 3) is the one representing best the interactions of archazolide with V-ATPase.

Docking Results for Derivatives 2−4. The docking of the archazolides derivatives **2**−**4** to the yeast c-ring model yielded similar results as for **1**. The five binding modes **B1**−**B5** are displayed also by derivatives **2**−**4** (Figure S14−S16), although with different populations. In agreement with the high activity of derivatives **2** and **3**, cluster **B5** is highly populated (Figure S17), probably due to a favorable interaction of the C1−C6 region with Y66. Thus, the relevance of the binding pose **B5** is confirmed by docking across the whole set of archazolide derivatives.

Refinement of Pose B5 by MD Simulations. To confirm the reliability of pose **B5**, the complexes of archazolide A (**1**)

dx.doi.org/10.1021/ci300242d | J. Chem. Inf. Model. 2012, 52, 2265−2272

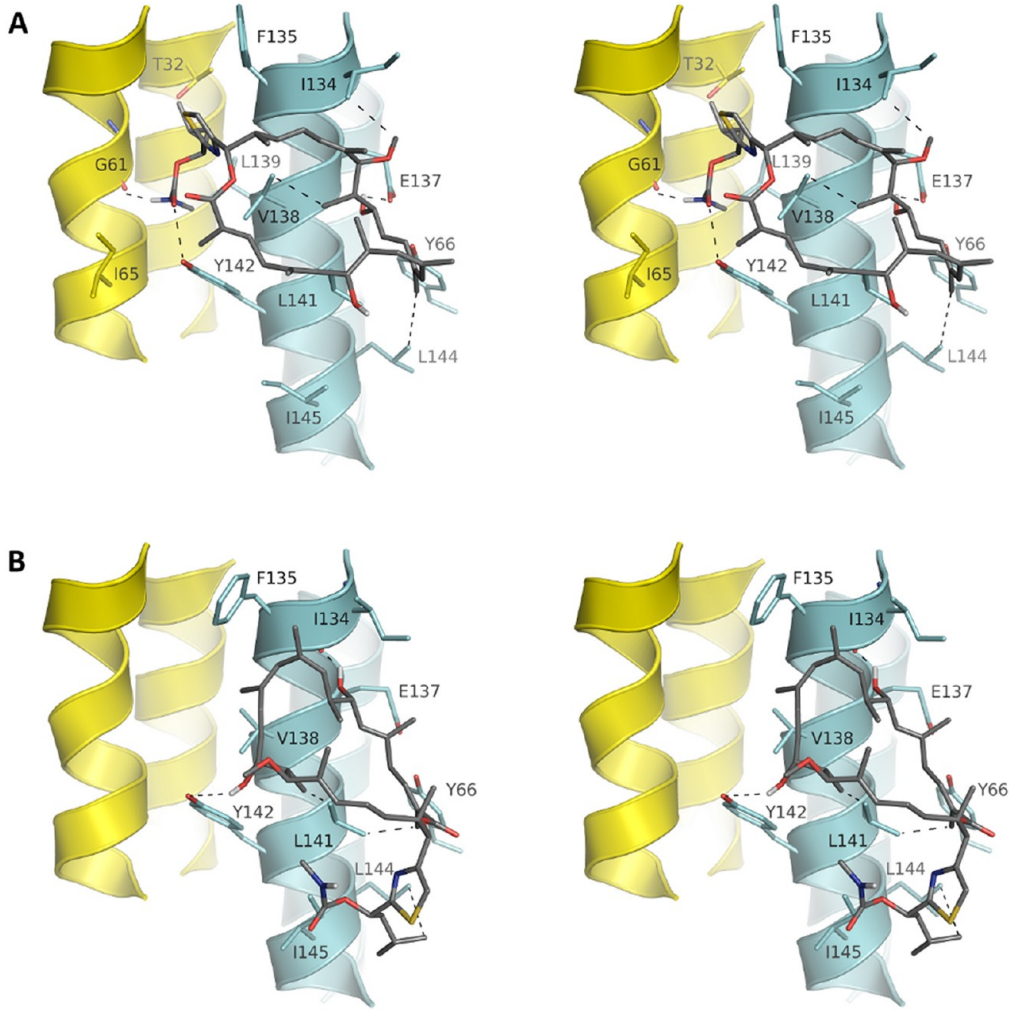

Figure 3. Stereoview of binding modes **B2** (**A**) and **B5** (**B**). Important residues belonging to one c subunit of the V_O-rotor protein are labeled in yellow and cyan, respectively. The ligand is shown in sticks (carbon: gray; oxygen: red; nitrogen: blue; sulfur: yellow; hydrogen: white). Key interactions are shown as dashed lines.

with the wild-type and the Y142N mutant of V-ATPase, corresponding to the binding pose **B5**, were refined during a short 3 ns MD simulation in an explicit phosphatidylethanolamine (PEA) membrane using the AMBER03[23] force field in the YASARA[24] molecular modeling program. Eight different sets of weak restraints were imposed in eight MD runs representing different combinations of contacts between the ligand and protein residues 134, 137, 142, and 144, as seen in binding pose **B5**. These residues were chosen because either biochemical data or molecular docking shows their interaction with the ligand (Table S1). To compare all 3 ns MD simulations, we monitored hydrogen bonds involving the C7-OH, the C15-OH, and the NH of the methyl carbamate side chain of archazolide. The conformation of the archazolide macrocycle remained stable during the MD run (Figure S18). As far as the interaction between archazolide and the binding site of DCCD around residues 134 and 137 is concerned, stable hydrogen bonds were formed between the C7-OH of the ligand and either the carbonyl backbone of I134 or the side chain of E137 in most of the runs. A hydrogen bond with the backbone of V138 was less frequently observed. If the C7-OH of archazolide forms a hydrogen bond to the carbonyl backbone of I134, the side chain of E137 interacts with the side chain of Y66. This hydrogen bond between the essential glutamate and the highly conserved adjacent tyrosine (Figure S2) is also present in the proton or sodium binding sites of F-ATPases.[25−27] The hydrogen bond between the C15-OH of archazolide and the side chain of residue 142 was observed considerably more often for the Y142N mutant than for the wild type protein (Table S2), in very good agreement with the higher affinity of archazolide for the mutant protein. Interestingly, the smaller asparagine side chain at position 142 favors the formation of the hydrogen bond between the methyl carbamate side chain of archazolide and the backbone of L141, which was observed more frequently for the Y142N mutant than for the wild type protein. In both MD runs a close interaction of the *i*-butyl side chain of archazolide and L144 was observed. Even when starting from another conformer of archazolide A, with a rotation of 180° around the $C-C_{Ar}$ bond in the archazolide side chain, the contact of the *i*-butyl group with L144 was restored during the MD run, in very good agreement with the sensitivity of the archazolide affinity for V-ATPase to mutations of L144.

The MD run with restraints set no. 3 for the wild type protein (Table S1) and the Y142N mutant (Table S2) was extended to 5 ns, and the snapshot of the trajectory with the

dx.doi.org/10.1021/ci300242d | J. Chem. Inf. Model. 2012, 52, 2265−2272

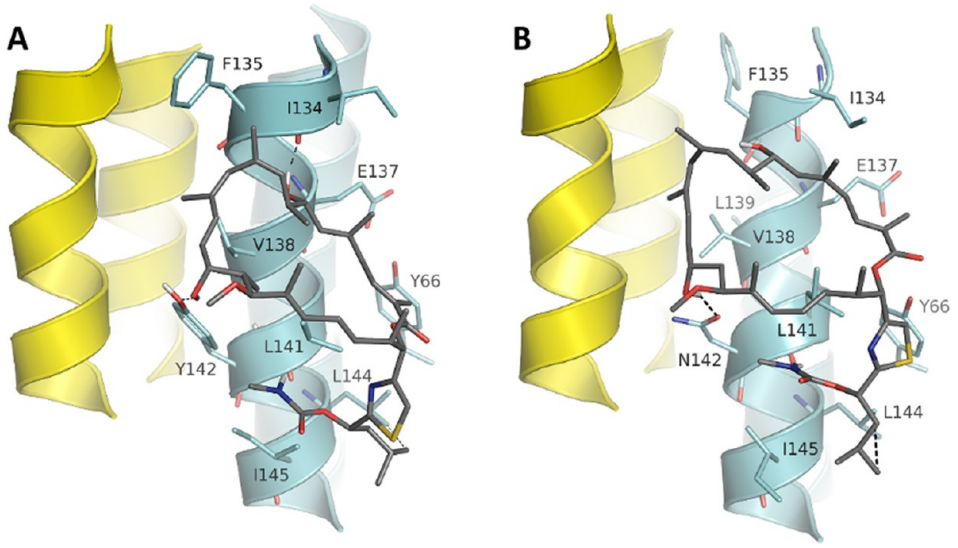

Figure 4. Lowest energy MD-refined binding mode **B5** to the wild type (**A**) and mutant Y142N (**B**) V-ATPase. Important residues belonging to one c subunit of the V_O-rotor protein are colored in yellow and cyan, respectively. The ligand is shown as sticks (carbon: gray; oxygen: red; nitrogen: blue; sulfur: yellow; hydrogen: white). Key interactions are shown as dashed lines.

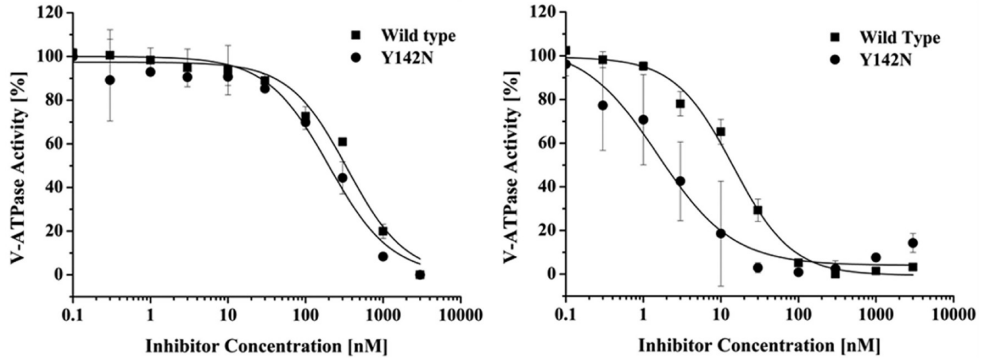

Figure 5. Influence of mutation Y142N in the yeast c subunit on the binding of ligand **4** (left) and ligand **5** (right). V-ATPase activities were measured on isolated yeast vacuoles of the wild type strain BMA64-1B and mutant strain Y142N.

lowest energy is shown in Figure 4. In essence, binding mode **B5** could be successfully refined by an MD simulation in an explicit membrane; the refined pose retains the essential protein–ligand interactions seen in docking and explains well the biochemical data available for the wild-type and mutant V-ATPases.

Experimental Validation of Binding Mode B5. The validity of binding mode **B5** was proved experimentally by testing the activity of archazolide analogs with mutant yeast V-ATPase. The distinctive landmark of **B5** is the positioning of the C15-OH next to Y142, in contrast to all other binding modes **B1**–**B4**, where the C15-OH is located close to I134, E137, and Y66. For archazolide A (**1**) previous studies showed that the Y142N mutant is ten times more sensitive to the ligand than the wild-type protein. If binding mode **B5** is correct, modifications at position C15 should promote a different behavior of the archazolide derivative with the Y142N mutant protein compared to the parental ligand **1**. Vice versa, if one of the other binding modes is correct, a ligand with modified C15-OH should behave like **1** with the Y142N mutant protein. Following this reasoning, we synthesized ligand **4**, which is dehydrogenated at C15 and tested its biological activity with both the wild type and the Y142N mutant protein. Interestingly, **4** shows similar inhibitory profiles for both the wild-type and mutant protein. This change of behavior with respect to the parental compound **1**, which is ten times more active toward the Y142N mutant V-ATPase, supports the vicinity of the C15-OH to Y142, thereby endorsing **B5** as a plausible binding mode (Figure 5). The increased activity of **1** with the Y142N mutant protein can be explained by an additional hydrogen bond formed between the hydroxyl group at C15 and the carbonyl group of the asparagine side chain in the Y142N mutant. This carbonyl group is a much better hydrogen bond acceptor than the hydroxyl group of the wild type tyrosine. In **4**, the oxidation of C15 leads to a sp^2-hybridization state, which, in conjunction to the triene system at C9–C14, stiffens the macrocycle of the ligand and likely results in an increased distance between the asparagine side chain of the Y142N mutant protein and the C15 carbonyl function. The absence of hydrogen bonds between the C15 functional group of ligand **4** and the residue 142 of the protein would explain the similar sensitivity of the wild type and the Y142N mutant protein to this ligand. Following the same reasoning, we expected that 1′-descarbamoyl-archazolide (**5**), which lacks the carbamate side chain, would show the same efficiency as **1** to the Y142N mutant proteins, since the hydroxyl function at C15 remains unmodified. This prediction is fully confirmed in bioactivity tests (Figure 5), showing an increased activity of ligand **5** toward mutant Y142N compared

dx.doi.org/10.1021/ci300242d | J. Chem. Inf. Model. 2012, 52, 2265–2272

to the wild type protein. Additionally, the lack of the side chain does not affect binding, since, in contrast to **B1**−**B4**, in **B5** the carbamate does not interact extensively with the protein. These data further support **B5** as the binding mode of archazolides to V-ATPases.

CONCLUSION

In this study, we describe the binding mode of archazolide A to the V-ATPAse using an interdisciplinary experimental and computational approach. We demonstrate that the functionality at C15 of the ligand is close to residue 142 of the protein, as shown by docking and confirmed by mutant cycle experiments. The conjugated region between C1 and C6 of the ligand is in proximity to the amino acids Y66 and E137, mainly entertaining hydrophobic interactions. This is consistent with the fact that the Y66F mutant binds archazolide A as strong as the wild-type protein. We observe a hydrogen bond between the hydroxyl group at C7 of archazolides and the backbone of residue I134, in full agreement with the loss of activity for archazolide C, with a bulky glucose moiety at C7, which would clash with the protein surface. The DCCD binding side is partially occupied by the archazolide, thereby preventing the binding of this V-ATPase inhibitor. Additionally, the binding pocket of the plecomacrolide inhibitors[17] is occupied too, which explains why archazolides compete with the binding of plecomacrolides to the V-ATPase.

Archazolides bind on the surface of the c ring rotor. While it is commonly assumed that ligands binding on the surface of the rotor exert their inhibitory activity by blocking the rotation, we notice that the interaction of archazolides with the essential glutamate could additionally prevent the E137-mediated proton exchange between the c ring rotor and subunit a. Both facts can rationalize the potent inhibitory effect of the V-ATPase function by archazolides.

In conclusion, here we present the first binding mode for the most potent V-ATPase inhibitor discovered so far. This binding mode, derived *in silico* and validated experimentally by mutant cycle experiments, explains well all previously existing SAR (Structure-Activity-Relationship) data. The next step along the way to promote archazolide-based ligands as therapeutic agents is the design of a simplified molecule, with an easy synthetic route that is capable of forming the same critical intermolecular interactions as the archazolide scaffold. Efforts in this direction are ongoing in our laboratories.

EXPERIMENTAL METHODS

Preparation of Protein Input Structures. The homology model of the yeast rotor was generated by aligning the amino acid sequence of the *S. cerevisiae* c subunit onto one of the 10-fold symmetric crystal structure of *E. hirae* (PDB-ID: 2BL2) and generating the homology model as described in ref 11. We then minimized the homology model using MacroModel9.7[28] and the OPLS2005[29] force field in aqueous solution and simplified the whole yeast rotor to three subunits for the docking (Figure S3). Protein side chain conformers were generated during a 1 ns MD simulation at 300 K at a constant pressure of 1 bar in the CHARMM22[30] force field with the CHARMM-XXL[31] program, using the TIP3P[32] model for water and restrained backbone (force constant of 1 kcal mol^{-1} $Å^{-2}$). Twenty snapshots were taken at equal time intervals of 50 ps each. To overcome clash barriers, we used a temperature gradient from 300 to 500 K for another 0.1 ns and extracted two additional snapshots at equal time intervals of 50 ps. For practical purposes, the resulting 22 conformers were then minimized in aqueous solution in MacroModel9.7[28] using OPLS2005[29] following the common procedure and served as protein input structures for the docking. While using different force fields may influence the outcome of the rotamer search, we do not expect a strong bias here given that modern protein force fields behave comparably with respect to structural and dynamical properties, as it has been shown by Price and Brooks.[33]

The mutant G61S was generated by substitution of residue 61 in the yeast homology model with serine, followed by minimization in the OPLS2005[29] force field in aqueous solution using Macromodel9.7.[28]

Molecular Docking. Archazolide A (**1**) and its derivatives (**2**−**4**) were docked to three subunits of the yeast homology model using Autodock3.0[21] with the Drugscore[22] scoring function. This combination has proven reliable for binding mode prediction in a "re-docking" evaluation.[34] Default parameters were used, except for the number of GA runs, which was set to 100, the population size, which was set to 200, and the number of generations, which was set to 50000. The search area and the electrostatic map size was chosen to be a cube with edge length of 22.7 Å (60 grid points, 0.375 grid point distance), centered on the triangle defined by amino acids E137, Y142, and L144 (Figure S9 and S10). The ligand macrocycle was kept fixed according to the experimentally determined conformation of archazolide A (**1**),[6] whereas the thiazole-bearing side chain and the methoxy- and the hydroxyl groups were fully rotatable throughout the docking. The structures of all archazolide derivatives (**2**−**4**) were generated in Maestro9.2 from the solution conformation for archazolide A (**1**). Subsequently, the modified regions were subjected to 100 steps of minimization with MacroModel9.7[28] using the OPLS2005[29] force field in aqueous solution, whereas the unmodified ones were frozen to the solution conformation of **1**. 2200 solutions were obtained for each archazolide analog (22 protein conformers × 100 docking poses). The 2200 structures were clustered at a ligand root mean squared deviation (rmsd) value of 2.0 Å. Clusters with population >5% (110 out of 2200 structures) were analyzed further. The structure with the lowest docking energy was regarded as cluster representative.

The solution conformation of archazolide A (**1**) was also docked to three subunits of the yeast mutant G61S using the same conditions, except that we did not create side chain conformers. 100 solutions were obtained (1 protein conformer × 100 docking poses), which were clustered at a ligand rmsd value of 2.0 Å. As shown in Figure S13 the population of binding modes **B1**−**B3** drops considerably upon substitution of G61, whereas **B5** comprises 70% of all solutions. The remaining 18 solutions are distributed among 7 other binding modes, with populations between 1 to 3 structures (data not shown).

Molecular Dynamics Simulations. The complexes of archazolide A and two variants of the V-ATPase protein (the wild type and the Y142N mutant) were refined in the YASARA program (YASARA Biosciences) using the AMBER03[23] force field with the TIP3P[32] model for water. The membrane used in the molecular dynamics simulations consisted of phosphatidylethanolamine lipids (PEA). The complexes were embedded into the membrane based on the location of hydrophobic residues.[24] The width and the position of the membrane were fitted to the data for the V-ATPase homologue of *E. hirae* (PDB-ID: 2BL2) deposited in the OPM database.[35] Force field

parameters for lipids and the ligand were derived using AutoSMILES.[36,37] The periodic box contained about 135000 atoms. The simulations were conducted at a constant temperature of 298 K using the Berendsen thermostat and a constant pressure of 1 bar. The simulation time step was set to 2.5 fs. During the first 0.25 ns of the MD simulation each of the complexes (wild-type and mutant) was kept frozen to allow the membrane to relax and to adapt to the embedded protein complex without disrupting its structure. During the next 3 ns of the simulation we imposed weak restraints on the experimentally predicted interactions between the ligand and residues 134, 137, 142, and 144 in the adjacent protein chain. Restraints were included in different combinations (Table S1 and S2): 1. hydrogen bond between the C7-OH of archazolide and the backbone or side chain of I134 and E137, respectively; 2. hydrogen bond between the C15-OH of archazolide and the side chain of Y142; 3. hydrophobic contact between the *i*-butyl side chain of archazolide and the side chain of I144. The restraints were imposed in the form of the SoftSquare potentials[38] (a hydrogen−acceptor distance equal to 2.0 ± 1 Å and for the van der Waals interaction with L144 a distance of: 3.0 ± 1.0 Å). We assessed the MD runs by monitoring hydrogen bond formation (Table S1 and S2). The hydrogen bonds statistics was computed using the VMD software[39] (donor−acceptor distance: 3.5 Å, angle cutoff: 30 degrees). The MD run with the restraints set no. 3 (Table S1 and S2) was extended to 5 ns, and the representative snapshot with the lowest energy was provided as a final result.

To check the stability of the V-ATPase model we further extended the MD simulation with restraints set no. 3 of the wild type protein to 10 ns and computed the rmsd with respect to the starting homology model (Figure S4).

Synthesis of Archazolide Derivatives. The structures of 15-dehydro-archazolide (**4**) and 1′-descarbamoyl-archazolide (**5**) were synthesized according to the published procedure.[10]

Biological Assays. Purification of yeast vacuoles and following activity assays were carried out as described in ref 11. The concentration of inorganic phosphate in the samples was determined according to ref 40.

■ ASSOCIATED CONTENT

Ⓢ Supporting Information

Protein sequence alignments, yeast homology model, electrostatics of yeast V-ATPase and archazolide A, computational details for the molecular docking as well as the molecular dynamics simulations, additional material of all docking-derived binding modes, and hydrogen bond analyses of the MD trajectories. This material is available free of charge via the Internet at http://pubs.acs.org.

■ AUTHOR INFORMATION

Corresponding Author

*Phone: +49 6221 3878552. Fax: +49 6221 3878519. E-mail: teresa.carlomagno@embl.de.

Present Addresses

[§]International Institute of Molecular and Cell Biology, 4 Ks. Trojdena, 02-109 Warsaw, Poland.

[▽]Kekulé-Institute of Organic Chemistry and Biochemistry, University Bonn.

Notes

The authors declare no competing financial interest.

■ ACKNOWLEDGMENTS

We thank the German Science Foundation (DFG, Graduate College 850:'Modeling of Molecular Properties') for generous financial support (stipend to S.D.) and cluster usage as well as Dennis Krüger, Alexander Metz, and Doris Klein (Heinrich-Heine-University Düsseldorf) for assistance in using Drugscore and fruitful discussions. T.C. acknowledges financial support from EMBL and Grant I/81 637 from the Volkswagen Stiftung. D.L. acknowledges the computational grant G35-6 from ICM Warsaw. S.B., M.H., and H.W. acknowledge financial support from the Volkswagen Stiftung (Grant I/82 801).

■ ABBREVIATIONS

DCCD = *N,N′*-dicyclohexylcarbodiimide; RDC = residual dipolar coupling; GA = genetic algorithm; MD = molecular dynamics; PEA = phosphatidylethanolamine

■ REFERENCES

(1) Sasse, F.; Steinmetz, H.; Höfle, G.; Reichenbach, H. Archazolids, new cytotoxic macrolactones from Archangium gephyra (Myxobacteria). Production, isolation, physico-chemical and biological properties. *J. Antibiot. (Tokyo)* **2003**, *56*, 520−525.

(2) Menche, D.; Hassfeld, J.; Steinmetz, H.; Huss, M.; Wieczorek, H.; Sasse, F. Archazolid-7-O-*β*-D-glucopyranoside − Isolation, Structural Elucidation and Solution Conformation of a Novel V-ATPase Inhibitor from the Myxobacterium Cystobacter violaceus. *Eur. J. Org. Chem.* **2007**, *2007*, 1196−1202.

(3) Menche, D.; Hassfeld, J.; Steinmetz, H.; Huss, M.; Wieczorek, H.; Sasse, F. The first hydroxylated archazolid from the myxobacterium Cystobacter violaceus: isolation, structural elucidation and V-ATPase inhibition. *J. Antibiot. (Tokyo)* **2007**, *60*, 328−331.

(4) Horstmann, N.; Essig, S.; Bockelmann, S.; Wieczorek, H.; Huss, M.; Sasse, F.; Menche, D. Archazolid A-15-O-beta-D-glucopyranoside and iso-archazolid B: potent V-ATPase inhibitory polyketides from the myxobacteria Cystobacter violaceus and Archangium gephyra. *J. Nat. Prod.* **2011**, *74*, 1100−1105.

(5) Hassfeld, J.; Fares, C.; Steinmetz, H.; Carlomagno, T.; Menche, D. Stereochemical determination of Archazolid A and B, highly potent vacuolar-type ATPase inhibitors from the Myxobacterium Archangium gephyra. *Org. Lett.* **2006**, *8*, 4751−4754.

(6) Fares, C.; Hassfeld, J.; Menche, D.; Carlomagno, T. Simultaneous determination of the conformation and relative configuration of archazolide a by using nuclear overhauser effects, J couplings, and residual dipolar couplings. *Angew. Chem., Int. Ed. Engl.* **2008**, *47*, 3722−3726.

(7) Huss, M.; Sasse, F.; Kunze, B.; Jansen, R.; Steinmetz, H.; Ingenhorst, G.; Zeeck, A.; Wieczorek, H. Archazolid and apicularen: novel specific V-ATPase inhibitors. *BMC Biochem.* **2005**, *6*, 13.

(8) Menche, D.; Hassfeld, J.; Li, J.; Rudolph, S. Total synthesis of archazolid A. *J. Am. Chem. Soc.* **2007**, *129*, 6100−6101.

(9) Menche, D.; Hassfeld, J.; Li, J.; Mayer, K.; Rudolph, S. Modular total synthesis of archazolid A and B. *J. Org. Chem.* **2009**, *74*, 7220−7229.

(10) Menche, D.; Hassfeld, J.; Sasse, F.; Huss, M.; Wieczorek, H. Design, synthesis and biological evaluation of novel analogues of archazolid: a highly potent simplified V-ATPase inhibitor. *Bioorg. Med. Chem. Lett.* **2007**, *17*, 1732−1735.

(11) Bockelmann, S.; Menche, D.; Rudolph, S.; Bender, T.; Grond, S.; von Zezschwitz, P.; Muench, S. P.; Wieczorek, H.; Huss, M. Archazolid A binds to the equatorial region of the c-ring of the vacuolar H+-ATPase. *J. Biol. Chem.* **2010**, *285*, 38304−38314.

(12) Beyenbach, K. W.; Wieczorek, H. The V-type H+ ATPase: molecular structure and function, physiological roles and regulation. *J. Exp. Biol.* **2006**, *209*, 577−589.

(13) Mandel, M.; Moriyama, Y.; Hulmes, J. D.; Pan, Y. C.; Nelson, H.; Nelson, N. cDNA sequence encoding the 16-kDa proteolipid of

chromaffin granules implies gene duplication in the evolution of H+-ATPases. *Proc. Natl. Acad. Sci. U.S.A.* **1988**, *85*, 5521−5524.
(14) Hinton, A.; Bond, S.; Forgac, M. V-ATPase functions in normal and disease processes. *Pflugers Arch.* **2009**, *457*, 589−598.
(15) Forgac, M. Vacuolar ATPases: rotary proton pumps in physiology and pathophysiology. *Nat. Rev. Mol. Cell Biol.* **2007**, *8*, 917−929.
(16) Finbow, M. E.; Eliopoulos, E. E.; Jackson, P. J.; Keen, J. N.; Meagher, L.; Thompson, P.; Jones, P.; Findlay, J. B. C. Structure of a 16 kDa integral membrane protein that has identity to the putative proton channel of the vacuolar H+-ATPase. *Protein Eng.* **1992**, *5*, 7−15.
(17) Bowman, B. J.; McCall, M. E.; Baertsch, R.; Bowman, E. J. A Model for the Proteolipid Ring and Bafilomycin/Concanamycin-binding Site in the Vacuolar ATPase of Neurospora crassa. *J. Biol. Chem.* **2006**, *281*, 31885−31893.
(18) Baker, N. A.; Sept, D.; Joseph, S.; Holst, M. J.; McCammon, J. A. Electrostatics of nanosystems: Application to microtubules and the ribosome. *Proc. Natl. Acad. Sci. U.S.A.* **2001**, *98*, 10037−10041.
(19) Erdélyi, M.; Pfeiffer, B.; Hauenstein, K.; Fohrer, J.; Gertsch, J.; Altmann, K.-H.; Carlomagno, T. Conformational Preferences of Natural and C3-Modified Epothilones in Aqueous Solution. *J. Med. Chem.* **2008**, *51*, 1469−1473.
(20) Marraud, M.; Aubry, A. Crystal structures of peptides and modified peptides. *Biopolymers* **1996**, *40*, 45−83.
(21) Morris, G. M.; Goodsell, D. S.; Halliday, R. S.; Huey, R.; Hart, W. E.; Belew, R. K.; Olson, A. J. Automated docking using a Lamarckian genetic algorithm and an empirical binding free energy function. *J. Comput. Chem.* **1998**, *19*, 1639−1662.
(22) Gohlke, H.; Hendlich, M.; Klebe, G. Knowledge-based scoring function to predict protein-ligand interactions. *J. Mol. Biol.* **2000**, *295*, 337−356.
(23) Duan, Y.; Wu, C.; Chowdhury, S.; Lee, M. C.; Xiong, G.; Zhang, W.; Yang, R.; Cieplak, P.; Luo, R.; Lee, T.; Caldwell, J.; Wang, J.; Kollman, P. A point-charge force field for molecular mechanics simulations of proteins based on condensed-phase quantum mechanical calculations. *J. Comput. Chem.* **2003**, *24*, 1999−2012.
(24) Krieger, E. 2003, YASARA (www.yasara.org/sd).
(25) Murata, T.; Yamato, I.; Kakinuma, Y.; Leslie, A. G. W.; Walker, J. E. Structure of the Rotor of the V-Type Na+-ATPase from Enterococcus hirae. *Science* **2005**, *308*, 654−659.
(26) Pogoryelov, D.; Yildiz, O.; Faraldo-Gomez, J. D.; Meier, T. High-resolution structure of the rotor ring of a proton-dependent ATP synthase. *Nat. Struct. Mol. Biol.* **2009**, *16*, 1068−1073.
(27) Meier, T.; Ferguson, S. A.; Cook, G. M.; Dimroth, P.; Vonck, J. Structural Investigations of the Membrane-Embedded Rotor Ring of the F-ATPase from Clostridium paradoxum. *J. Bacteriol.* **2006**, *188*, 7759−7764.
(28) Macromodel, version 9.7; Schrödinger, LLC: New York, NY, 2009.
(29) Jorgensen, W. L.; Maxwell, D. S.; Tirado-Rives, J. Development and Testing of the OPLS All-Atom Force Field on Conformational Energetics and Properties of Organic Liquids. *J. Am. Chem. Soc.* **1996**, *118*, 11225−11236.
(30) MacKerell, A. D.; et al. All-Atom Empirical Potential for Molecular Modeling and Dynamics Studies of Proteins. *J. Phys. Chem. B* **1998**, *102*, 3586−3616.
(31) Chemistry at HARvard Macromolecular Mechanics (CHARMM), version 35b2, 2008.
(32) Jorgensen, W. L.; Chandrasekhar, J.; Madura, J. D.; Impey, R. W.; Klein, M. L. Comparison of simple potential functions for simulating liquid water. *J. Chem. Phys.* **1983**, *79*, 926−935.
(33) Price, D. J.; Brooks, C. L. Modern protein force fields behave comparably in molecular dynamics simulations. *J. Comput. Chem.* **2002**, *23*, 1045−1057.
(34) Sotriffer, C. A.; Gohlke, H.; Klebe, G. Docking into Knowledge-Based Potential Fields: A Comparative Evaluation of DrugScore. *J. Med. Chem.* **2002**, *45*, 1967−1970.
(35) Lomize, M. A.; Pogozheva, I. D.; Joo, H.; Mosberg, H. I.; Lomize, A. L. OPM database and PPM web server: resources for positioning of proteins in membranes. *Nucleic Acids Res.* **2012**, *40* (D1), D370−D376.
(36) Jakalian, A.; Jack, D. B.; Bayly, C. I. Fast, efficient generation of high-quality atomic charges. AM1-BCC model: II. Parameterization and validation. *J. Comput. Chem.* **2002**, *23*, 1623−1641.
(37) Wang, J.; Wolf, R. M.; Caldwell, J. W.; Kollman, P. A.; Case, D. A. Development and testing of a general amber force field. *J. Comput. Chem.* **2004**, *25*, 1157−1174.
(38) Brunger, A. T. *X-PLOR version 3.1: A System for X-ray Crystallography and NMR*; Yale University Press: New Haven, CT, 1993.
(39) Humphrey, W.; Dalke, A.; Schulten, K. VMD: Visual molecular dynamics. *J. Mol. Graphics Modell.* **1996**, *14*, 33−38.
(40) Wieczorek, H.; Cioffi, M.; Klein, U.; Harvey, W. R.; Schweikl, H.; Wolfersberger, M. G. Isolation of goblet cell apical membrane from tobacco hornworm midgut and purification of its vacuolar-type ATPase. In *Methods Enzymology*; Sidney Fleischer, B. F., Ed.; Academic Press: 1990; Vol. *192*, pp 608−616.